3-D-Printed E-Band Compressive Horn Antenna for High-Sensing-Capacity Imaging Applications

Ali Molaei, Anthony Bisulco, Luis Tirado, Alexander Zhu, Diego Cachay, Ashkan Ghanbarzadeh Dagheyan, and Jose Martinez-Lorenzo, *Senior Member, IEEE*

***Abstract*—Spectral coding is of special interest in high-sensing-capacity imaging applications. This letter presents the design, fabrication, and experimental validation of a lightweight and robust 3-D-printed compressive horn antenna, capable of performing spectral coding for such applications. First, a pyramidal horn antenna is designed to operate within the E-band. Then, a dielectric piece with a pseudorandom geometric pattern is inserted inside the horn to distort the radiation pattern of the antenna in both near- and far-field regions. The performance of both antennas is evaluated by their return loss and radiation patterns.**

***Index Terms*—Compressive antenna, high-sensing-capacity, millimeter-wave (mm-wave) antenna, pyramidal horn antenna (PHA), 3-D printing.**

I. Introduction

TRANSMITTING and receiving antenna modules that are being used in conventional imaging systems have radiation patterns that do not change significantly over the operational frequency band (spectral domain). They also usually have a directional main lobe in the boresight or endfire axis (spatial domain) of the antenna [1]. In other words, they do not take into consideration that consecutive measurements at different frequencies for different antenna elements contain similar information. However, antennas used in sensing applications can be engineered to compress the transmitting and receiving data.

Several groups have recently proposed imaging systems with the aim of maximizing the information transfer efficiency, also known as the systems sensing capacity, between the imaging domain and the radar sensors [2]–[8]. For example, in [2], a spatially dependent compressive reflector antenna (CRA) is presented to enhance the sensing capacity of a millimeter-wave (mm-wave) radar system. The proposed CRA spatially codes the electromagnetic field in the imaging domain, while in [7], the CRA is used to code the electromagnetic field in the spectral domain. Notwithstanding, both designs use a large aperture to code the electromagnetic field. In this letter, we have aimed to reduce the hardware complexity of the CRA, shifting the spectral coding burden to the 3-D-printed feeding antenna elements of the reflector.

Additive manufacturing, or 3-D printing, refers to the process of building a component by depositing successive layers of materials, such as plastic or metal. Recently, 3-D printing has been introduced as a feasible alternative to traditional mechanical fabrication techniques for microwave [9]–[11] and mm-wave [12]–[16] antenna applications due to its cost-effective, rapid, lightweight, and robust manufacturing.

This letter describes the design, fabrication, and experimental validation of a small, low-cost, and lightweight 3-D-printed compressive horn antenna (CHA), which may be used to enable spectral coding in high-sensing-capacity mm-wave imaging applications. The CHA is built by inserting a dielectric with a pseudorandom geometric pattern in the aperture of a 3-D-printed pyramidal horn antenna (PHA). The performance of the antenna is evaluated in terms of its near- and far-field radiation pattern and return loss.

II. Antenna Design and Fabrication

A. Pyramidal Horn Antenna

The PHA has been investigated thoroughly in literature [17], and some general design modifications are described in [18] and [19]. The design presented here targets the E-band and is composed of a pyramidal horn connected to a WR-12 rectangular waveguide interface with a UG-387/U flange. Fig. 1(a) and (b) shows the geometry of the proposed PHA. The antenna is simulated using the commercial finite-element-analysis method software HFSS. It is modeled using 50 μm of silver on top of a 2.4 mm thick VeroWhitePlus dielectric material with a relative permittivity of $\epsilon_r = 2.8$ and a dielectric loss tangent of $\tan\delta = 0.04$. The dielectric serves only as a supportive structure for the silver layer.

For fabrication purposes, the antenna model is split into two assembly pieces to facilitate the metalization process. Alignment pins and snug fit holes are configured on each split piece

Manuscript received February 3, 2018; revised June 7, 2018; accepted July 3, 2018. Date of publication July 25, 2018; date of current version August 31, 2018. This work was supported in part by the U.S. Department of Homeland Security under Award 2013-ST-061-ED0001 and in part by the National Science Foundation CAREER program under Award 1653671. *(Corresponding author: Jose Martinez-Lorenzo.)*

A. Molaei, A. Bisulco, and L. Tirado are with the Department of Electrical and Computer Engineering, Northeastern University, Boston, MA 02115 USA (e-mail: molaei.a@husky.neu.edu; bisulco.a@husky.neu.edu; tirado.l@husky.neu.edu).

A. Zhu is with the Wayland High School, Wayland, MA 01778 USA (e-mail: azuzhu2000@gmail.com).

D. Cachay is with the Boston Latin School, Boston, MA 02115 USA (e-mail: diegocachay@gmail.com).

A. Ghanbarzadeh Dagheyan is with the Department of Mechanical and Industrial Engineering, Northeastern University, Boston, MA 02115 USA (e-mail: ghanbarzadehdaghe.a@husky.neu.edu).

J. Martinez-Lorenzo is with the Department of Electrical and Computer Engineering and the Department of Mechanical and Industrial Engineering, Northeastern University, Boston, MA 02115 USA (e-mail: j.martinez-lorenzo@neu.edu).

Digital Object Identifier 10.1109/LAWP.2018.2859912

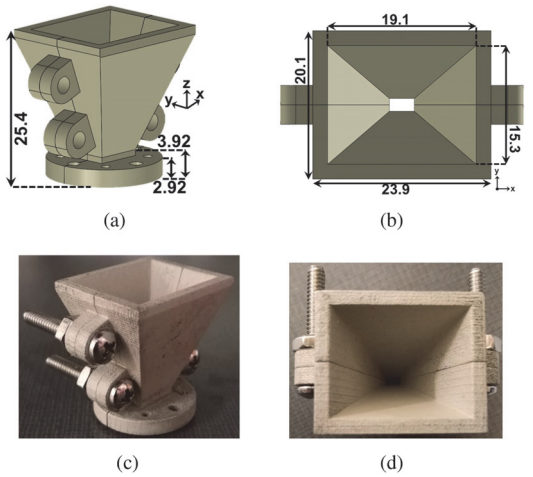

Fig. 1. Geometry of the designed E-band PHA. (a) Perspective view and (b) top view of the CAD model. (c) Perspective view and (d) top view of the fabricated model. All dimensions are in millimeters.

to ensure that there is no misalignment when the pieces are integrated. The computer-aided design (CAD) models are fabricated by an Objet Eden 260VS 3-D printer with VeroWhitePlus as the filament material. Then, the printed pieces are metalized using an acrylic-based silver conductive coating spray (842AR–SUPER SHIELD). Each piece is sprayed three times with a 5 min break between each spray to avoid trapping solvents between the coats. The pieces are then cured at room temperature for 45 min. Finally, antenna pieces are assembled with the alignment pins and fixed by $\#4 - -40$ bolts and nuts. Fig. 1(c) and (d) shows the perspective and top views of the fabricated PHA, respectively.

B. Compressive Horn Antenna

The design of the PHA can be customized in order to build a CHA [see Fig. 2(a) and (b)] with spectral coding capabilities. For this purpose, a pseudorandom dielectric structure is 3-D printed and inserted into the PHA. The pseudorandom structure is built using the same VeroWhitePlus material used for printing the PHA; it has a relative permittivity of $\epsilon_r = 2.8$ and a dielectric loss tangent of $\tan\delta = 0.04$. The pseudorandom structure is designed using a MATLAB code that pseudorandomly places 2 mm $\times$ 2 mm $\times$ 2 mm dielectric voxels inside a 20 mm $\times$ 16 mm $\times$ 14 mm volumetric region. The code uses a Bernoulli distribution to determine whether a voxel is filled with a dielectric material or not, where each outcome has equal probability $p = 0.5$. Moreover, an additional constraint is used to ensure that each voxel is connected to at least one face of another voxel in the space, thus resulting in a single united piece. Finally, the CAD model of the dielectric structure is cut to freely fit inside the PHA. Fig. 2(c) and (e), respectively, shows the CAD model and the fabricated pseudorandom dielectric piece. Alignment pins and snug fit holes are added to the horn and the dielectric piece, respectively, to fix the inserted dielectric inside the horn. Fig. 2(d) and (f) shows the pseudorandom model inserted into the aperture of the horn. One of the top split assembly parts is removed in these figures to have a better visual view of the integrated part.

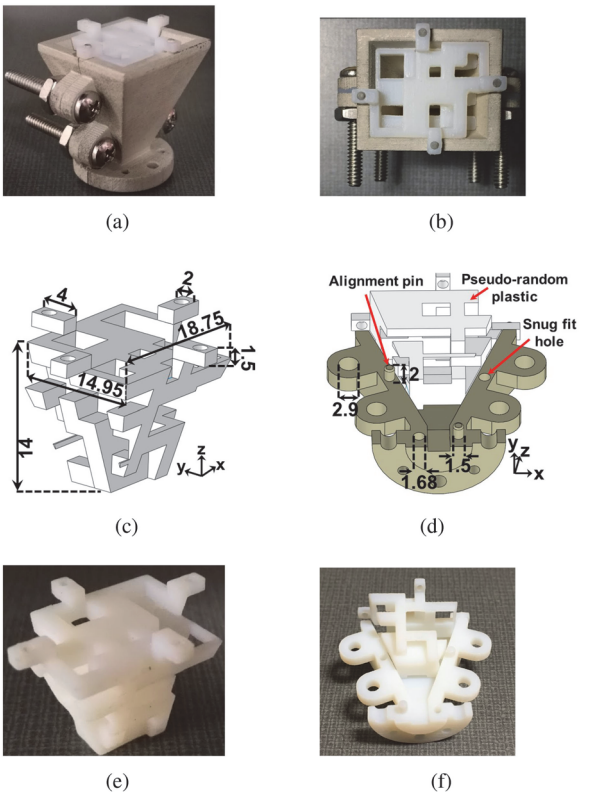

Fig. 2. (a) CAD and (c) fabricated model of the designed pseudorandom plastic piece. (b) CAD and (d) fabricated model of the pseudorandom plastic piece inserted inside the printed horn. One of the horn split assembly parts is removed to have a better visual view of the integrated part. (e) Perspective view and (f) top view of the fabricated CHA. All dimensions are in millimeters.

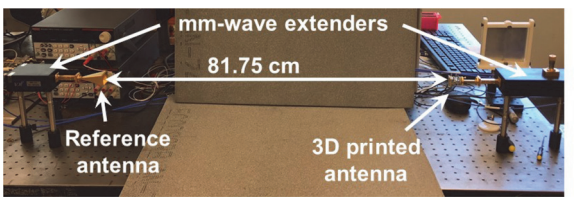

Fig. 3. Experimental setup for measuring the boresight gain and return loss of the fabricated antennas.

III. Results

Fig. 3 shows the experimental setup for measuring the boresight gain of the PHA. Measurements are performed using the N5242A PNA-X Network Analyzer equipped with VDI mm-wave extender modules. The printed antenna is mounted on the transmit side of the setup. The receiving antenna is a Millitech standard gain pyramidal horn (SGH-12-RP000). The PHA has a boresight gain varying from 15 to 20 dB in the E-band, with a value equal to 18 dB at the center frequency (75 GHz). Compared to the simulation results, the fabricated antenna shows about 3 dB less gain. This could be due to the impurity of the silver spray, which reduces its conductivity. There are two other possible reasons to explain the reduced gain of the fabricated antenna when compared to the simulation. First, coating each one of the WR-12 waveguides with the metallic paint results in slightly rounded edges, and second, the mechanical

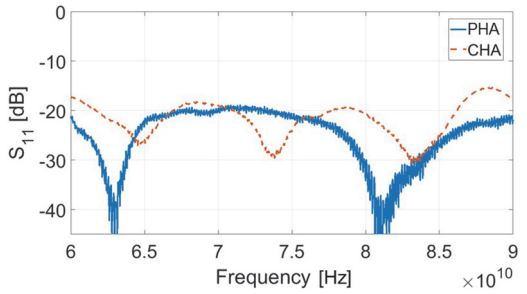

Fig. 4. Measured S_{11} for the fabricated PHA and CHA.

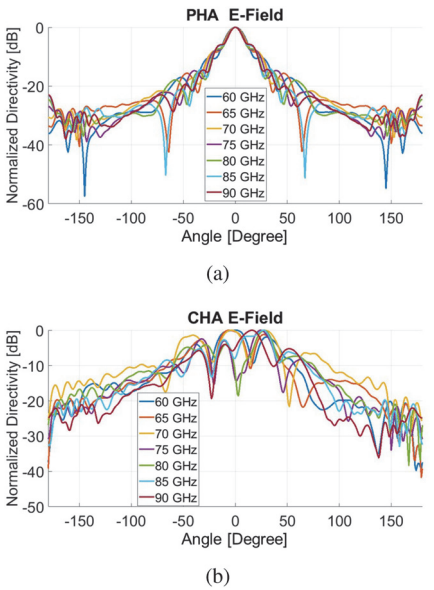

Fig. 5. E-Plane far-field graphs. (a) PHA E-field. (b) CHA E-field.

alignment of the top pieces introduces certain nonuniformity at their intersection. These make the wave propagation through the 3-D-printed WR-12 waveguide maybe present additional losses, thus presenting additional gain degradation.

The performance of the presented CHA is studied in terms of S_{11}, as well as near- and far-field radiation patterns, and then compared with those of the PHA. As shown in Fig. 4, both the CHA and the PHA have a return loss better than 16 dB within the frequency range of 60–90 GHz. Figs. 5 and 6, respectively, compare the E-plane and H-plane normalized radiation patterns of the PHA and CHA. Also, the near field of the antennas is plotted in Fig. 7 at 60 GHz [see Fig. 7(b) and (c)], 75 GHz [see Fig. 7(d) and (e)], and 90 GHz [see Fig. 7(f) and (g)]. As can be seen from both the near- and far-field plots, the radiation pattern of the CHA varies with frequency, while for the PHA, these patterns remain fairly consistent. This unique feature of the CHA can be used to enable spectral coding in near- or far-field imaging applications.

To validate the performance of the 3-D-printed horn antennas, near-field measurements for both the PHA and the CHA are performed, and the results are compared with those of the simulations. For this purpose, the magnitude and phase of E_y are measured on a 2-D plane in front of the antenna, as shown in Fig. 8(a). The simulated and measured near fields of the

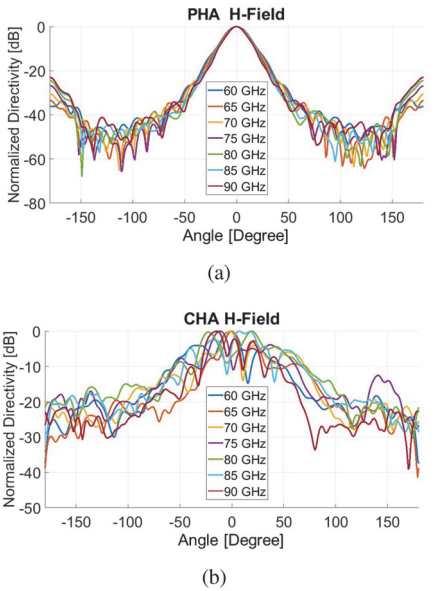

Fig. 6. H-plane far-field graphs. (a) PHA H-field. (b) CHA H-field.

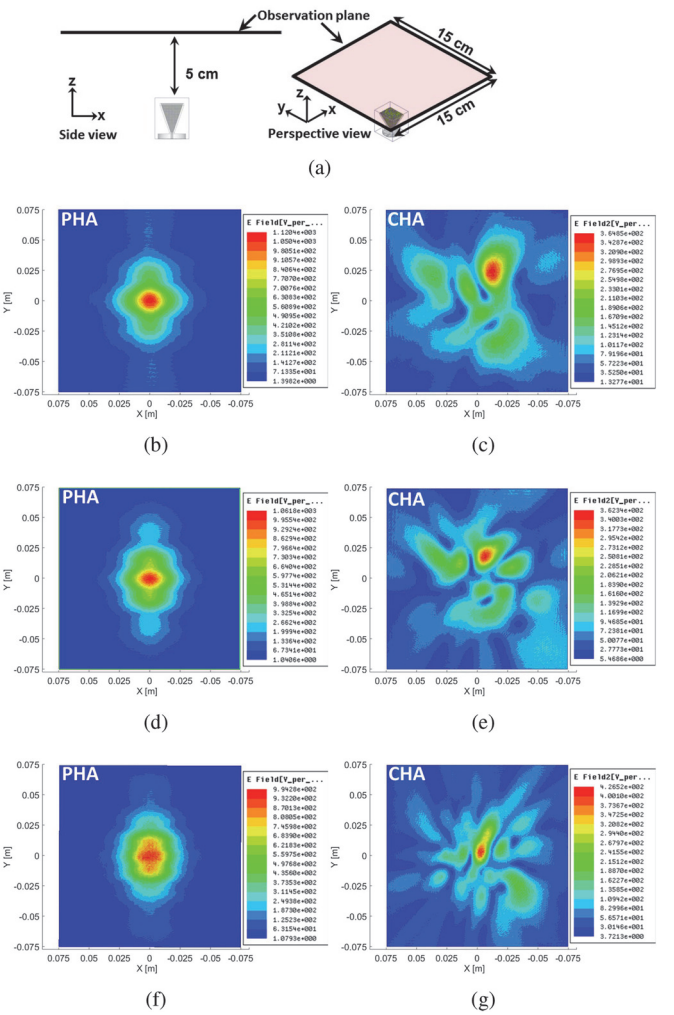

Fig. 7. Magnitude of E-field in near field of the antennas. (a) E-fields are plotted on a 15 cm × 15 cm plane, which is 5 cm far from the antennas. The fields are plotted at (b) and (c) 60 GHz; (d) and (e) 75 GHz; and (f) and (g) 90 GHz.

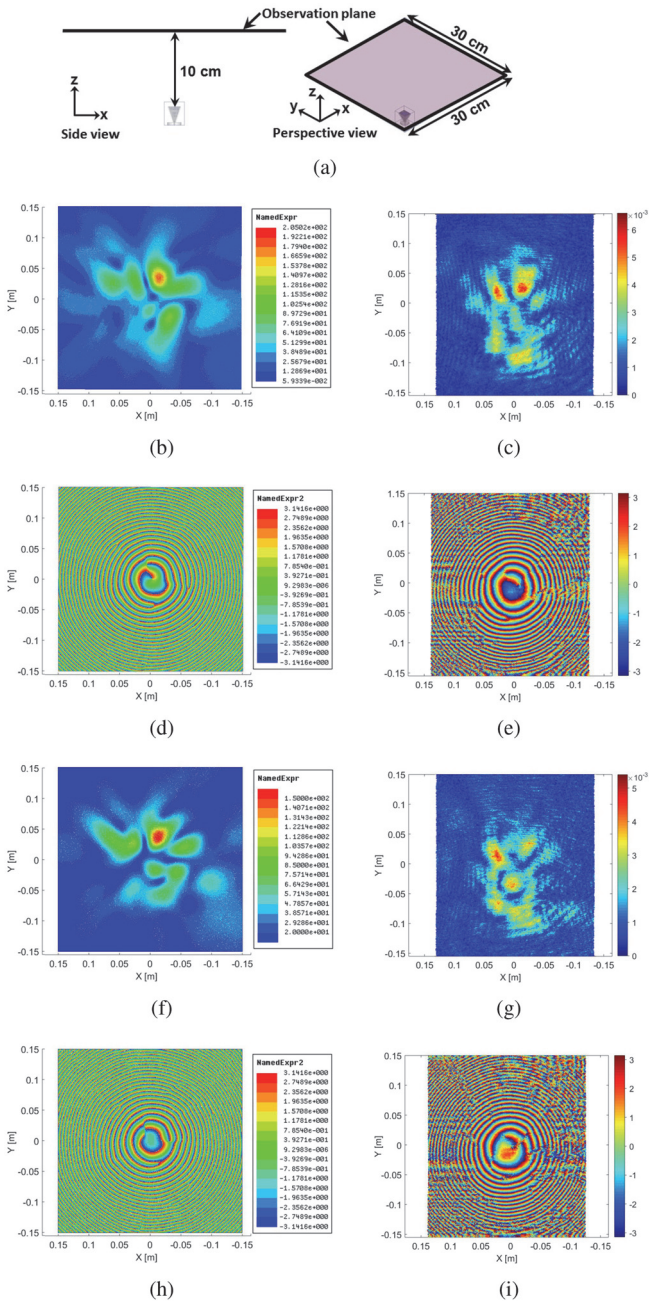

Fig. 8. (left) Simulated and (right) measured near field of the CHA. The E-fields are plotted on a 30 cm $\times$ 30 cm plane, which is 10 cm far from the antenna. The magnitude of the E_y is plotted at (a) and (b) 71.66 GHz and (e) and (f) 75.20 GHz. The phase of the E_y is plotted at (c) and (d) 71.66 GHz and (g) and (h) 75.20 GHz.

CHA are plotted in Fig. 8 for 71.66 and 75.2 GHz. As it can be seen from these two figures, the measurements follow well the simulation results.

IV. Conclusion

This letter presented the design, fabrication, and experimental validation of a low-cost and lightweight CHA. The CHA is built by customizing the design of the PHA to perform spectral coding in the E-band. Additive manufacturing or 3-D printing is used to fabricate the antennas. The CHA has the ability to create spectral codes in the near and far fields of the antenna. This would be especially useful for sensing and imaging applications with high-sensing-capacity requirements. Here, a quantitative analysis of the spectral coding efficiency (or sensing capacity [2]) and imaging performance of the CHA have not been addressed, given its dependence on the location of the antennas and the imaging region. However, this will be done in the future by building an imaging system that uses CHAs as sensing elements.

References

[1] S. S. Ahmed, A. Schiess, and L.-P. Schmidt, "Near field mm-wave imaging with multistatic sparse 2D-arrays," in *Proc. Eur. Radar Conf.*, 2009, pp. 180–183.

[2] J. Martinez-Lorenzo, J. Heredia Juesas, and W. Blackwell, "A single-transceiver compressive reflector antenna for high-sensing-capacity imaging," *IEEE Antennas Wireless Propag. Lett.*, vol. 15, pp. 968–971, 2016.

[3] A. Molaei, J. H. Juesas, and J. A. M. Lorenzo, "Compressive reflector antenna phased array," in *Antenna Arrays and Beam-Formation*. Rijeka, Croatia: InTech, 2017.

[4] D. R. Smith *et al.*, "Security screening via computational imaging using frequency-diverse metasurface apertures," *Proc. SPIE*, vol. 10189, 2017, Art. no. 101890B.

[5] T. A. Sleasman, M. F. Imani, M. Boyarsky, J. Gollub, and D. R. Smith, "Reconfigurable metasurface apertures for computational imaging," *Proc. Math. Imag. Conf.*, 2017, Paper MM2C.4.

[6] J. H. Juesas, A. Molaei, L. Tirado, W. J. Blackwell, and J. A. Martinez-Lorenzo, "Norm-1 regularized consensus-based ADMM for imaging with a compressive antenna," *IEEE Antennas Wireless Propag. Lett.*, vol. 16, pp. 2362–2365, 2017.

[7] A. Molaei, J. Heredia-Juesas, and J. Martinez-Lorenzo, "A 2-bit and 3-bit metamaterial absorber-based compressive reflector antenna for high sensing capacity imaging," in *Proc. IEEE Int. Symp. Technol. Homeland Secur.*, 2017, pp. 1–6.

[8] A. Molaei, G. Ghazi, J. Heredia-Juesas, H. Gomez-Sousa, and J. Martinez-Lorenzo, "High capacity imaging using an array of compressive reflector antennas," in *Proc. 11th IEEE Eur. Conf. Antennas Propag.*, 2017, pp. 1731–1734.

[9] J. Tak, D.-G. Kang, and J. Choi, "A lightweight waveguide horn antenna made via 3D printing and conductive spray coating," *Microw. Opt. Technol. Lett.*, vol. 59, no. 3, pp. 727–729, 2017.

[10] J. S. Silva *et al.*, "Stereolithography-based antennas for satellite communications in Ka-band," *Proc. IEEE*, vol. 105, no. 4, pp. 655–667, Apr. 2017.

[11] J.-C. S. Chieh, B. Dick, S. Loui, and J. D. Rockway, "Development of a Ku-band corrugated conical horn using 3-D print technology," *IEEE Antennas Wireless Propag. Lett.*, vol. 13, pp. 201–204, 2014.

[12] B. Zhang and H. Zirath, "A metallic 3-D printed E-band radio front end," *IEEE Microw. Wireless Compon. Lett.*, vol. 26, no. 5, pp. 331–333, May 2016.

[13] B. Zhang, P. Linnér, C. Karnfelt, P. L. Tarn, U. Södervall, and H. Zirath, "Attempt of the metallic 3D printing technology for millimeter-wave antenna implementations," in *Proc. IEEE Asia-Pacific Microw. Conf.*, 2015, vol. 2, pp. 1–3.

[14] E. Köhler, S. Rahiminejad, and P. Enoksson, "Evaluation of 3D printed materials used to print WR10 horn antennas," *J. Phys.: Conf. Ser.*, vol. 757, 2016, Art. no. 012026.

[15] E. Menargues *et al.*, "Polymer-based metal coated additive manufactured V-and W-band antenna feed chain components," in *Proc. 11th Eur. Conf. Antennas Propag.*, 2017, pp. 584–588.

[16] A. Bisognin *et al.*, "3D printed plastic 60 GHz lens: Enabling innovative millimeter wave antenna solution and system," in *Proc. IEEE MTT-S Int. Microw. Symp.*, 2014, pp. 1–4.

[17] W. L. Stutzman and G. A. Thiele, *Antenna Theory and Design*. New York, NY, USA: Wiley, 2012.

[18] X. Li, S. C. Hagness, M. K. Choi, and D. W. van der Weide, "Numerical and experimental investigation of an ultrawideband ridged pyramidal horn antenna with curved launching plane for pulse radiation," *IEEE Antennas Wireless Propag. Lett.*, vol. 2, pp. 259–262, 2003.

[19] R. Dehdasht-Heydari, H. R. Hassani, and A. R. R. Mallahzadeh, "Quad ridged horn antenna for UWB applications," *Prog. Electromagn. Res.*, vol. 79, pp. 23–38, 2008.